Research Network FWF S105

Photoacoustic Imaging in Medicine and Biology

http://pai.uibk.ac.at

Impedance-Acoustic Tomography

B. Gebauer and O. Scherzer

August 2008

PAI Report No. 2

FWF Der Wissenschaftsfonds.

universität innsbruck

IMPEDANCE-ACOUSTIC TOMOGRAPHY

BASTIAN GEBAUER[†] AND OTMAR SCHERZER[‡]

Abstract. In this work we present a new hybrid imaging technique that combines electrical impedance tomography with acoustic tomography. The novel technique makes use of the fact that the absorbed electrical energy inside the body raises its temperature, thus leading to expansion effects. The expansion then induces an acoustic wave which can be recorded outside the body and consequently be used to calculate the absorbed energy inside the body from which the electrical conductivity can be reconstructed. In other words we try to combine the high contrast of EIT with the high resolution of ultrasound.

1. Introduction. In electrical impedance tomography (EIT) an electrical voltage $f(x)$ is applied to the surface S of a body B, thus giving rise to an electrical potential $u(x)$ inside the body. One then measures the resulting surface current j and tries to reconstruct the conductivity inside the body from one or several voltage-current pair(s) $(f(x), j(x))$ on the boundary.

The problem is known to be severely ill-posed and though a number of commercial EIT systems exists a stable reconstruction algorithm still seems to be out of reach. As a starting point for the interested reader we refer to the survey articles of Cheney, Isaacson and Newell [7], Borcea [4, 5], Lionheart [19] and Bayford [3]. A recent study reporting on the high permittivity and conductivity contrast of different breast tissues over the frequency range 40Hz–100MHz can be found in Stoneman, et al, [27]. It has to be noted, however, that the conductivity value alone does not seem to be a sufficient criterion to distinguish cancerous from healthy breast tissue, cf. also the studies of Lazebnik, et al, [16, 17] for the microwave frequency range from 0.5 to 20GHz.

A promising approach to overcome the intrinsic ill-posedness of the problem is to combine electrical impedance tomography with another imaging system that provides additional information. The most prominent example is magnetic resonance electrical impedance tomography (MREIT), that combines EIT with measurements of the magnetic flux from which one obtains the current density *inside* the body, cf., the works of Kwon, Woo, Yoon and Seo [14], S. Kim, Kwon, Seo and Yoon [12], Y. J. Kim, Kwon, Seo and Woo [11] and the recent work of Nachman, Tamasan and Timonov [22]. Another approach is magnetoacoustic imaging where an exterior magnetic field is used to generate displacements in the body via the Lorentz force. The resulting pressure wave is measured by ultrasound transducers and provides information about the interior current density, cf., e.g., Ma and He [20] and the preprint [2] of Ammari, Capdeboscq, Kang and Kozhemyak for recent references. Independently of this work, Ammari, Bonnetier, Capdeboscq, Tanter and Fink have recently proposed to use ultrasound to produce localized elastic perturbations to locally change the conductivity inside a body, cf. [1]. From the resulting change in the EIT-measurements they obtain the energy density inside the body and use this additional information to reconstruct the conductivity.

[†]Institut für Mathematik, Johannes Gutenberg-Universität, 55099 Mainz, Germany
gebauer@math.uni-mainz.de

[‡]Department of Computer Science, University of Innsbruck, Technikerstr. 21a, 6020 Innsbruck, Austria
otmar.scherzer@uibk.ac.at, http://informatik.uibk.ac.at/infmath

In this work we propose a new method to obtain additional interior information for electrical impedance tomography by combining it with ultrasound tomography. Similarly to magnetoacoustic imaging we obtain our additional information from creating a pressure wave inside the body. However, we do not rely on an externally applied magnetic field and the Lorentz force but on thermal expansion. The resulting additional interior information is the same that Ammari et al. obtain by elastic deformations, i.e., the interior energy density.

To be more specific, we will make use of the fact that the absorbed energy inside the body raises its temperature, thus leading to expansion effects. The expansion then induces an acoustic wave which can be recorded outside the body and consequently be used to calculate the absorbed energy inside the body. The advantage of using acoustical rather than electromagnetic measurements for the reconstruction is that we can then choose the excitation frequency small with respect to the speed of electromagnetic waves (so that the model of impedance tomography holds true) but large with respect to the speed of sound (so that the we obtain a high resolution in the reconstructions). In other words we try to combine the high contrast of EIT with the high resolution of ultrasound. The ideas for this combination stem from thermoacoustic computerized tomography where a body is illuminated and thus heated up with a short pulse of light and the resulting acoustic pressure wave is recorded. For an introduction into the field of thermoacoustic tomography we refer to the recent special section in the journal Inverse Problems [23]. A survey on experimental setups for thermoacoustic imaging can be found in Xu and Wang [28].

The outline of this work is as follows. We start by developing the model of impedance-acoustic tomography in Section 2.1 and study the well-posedness of the resulting direct problem in 2.2. In Section 3 we study the associated inverse problems and derive first reconstruction algorithms. Finally we show a preliminary numerical examples for the simulation of impedance-acoustic tomography as well as for the reconstruction algorithms in Section 4.

2. Impedance-acoustic computerized tomography.

2.1. Derivation of the modeling equations. If a stationary electrical voltage $f(x)$ is applied to the surface S of a body $B \subset \mathbb{R}^n$, $n = 2$ or $n = 3$, this gives rise to an electrical potential $u(x)$ inside the body. In the state of equilibrium the potential is given by the solution u of

$$\nabla \cdot (\sigma(x)\nabla u(x)) = 0 \qquad \text{in } B, \tag{2.1}$$

$$u(x)|_S = f(x) \qquad \text{on } S, \tag{2.2}$$

where $\sigma(x)$ is the specific conductivity of the body. One can then measure the resulting surface current

$$j(x) = \sigma(x)\partial_\nu u(x)|_S$$

($\nu = \nu(x)$ is the outer normal vector at a surface point $x \in S$) and try to reconstruct $\sigma(x)$ from one or several voltage-current pair(s) $(f(x), j(x))$.

An electrical potential almost instantly reaches its state of equilibrium, so that if we apply a time-dependent voltage $F(x,t) = f(x)\sqrt{g(t)}$ that varies slowly in time (compared to the speed of electromagnetic waves) the induced electric potential is given by its quasi-statical limit $U(x,t) = u(x)\sqrt{g(t)}$, where $u(x)$ solves (2.1),(2.2).

(We choose the notation $\sqrt{g(t)}$ in order to have g proportional to the amount of applied electrical power in equation (2.3) below.)

When electrical currents are flowing through a body three effects can be observed, stimulation of nerves, electrolysis and thermal heating, cf. e.g. [9]. We concentrate on the heating effect and suggest to use high frequency currents, which have less stimulating effects on the nerves. Indeed, the effect of thermal heating with high frequency currents is exploited in *high frequency surgery*, cf. e.g. [9].

We will make use of the usual convention that "∇" and "Δ" are taken only with respect to spatial variables and that first, resp., second partial time-derivatives are denoted by one, resp., two dots. *Joule's law* describes the relation between the rate of variation of energy Q, i.e. the absorbed electrical power density $\dot{Q}(x,t)$, and the electric potential by

$$\dot{Q}(x,t) = \sigma(x)|\nabla U(x,t)|^2 = \sigma(x)|\nabla u(x)|^2 g(t). \tag{2.3}$$

If the voltage is only applied for a short time we can neglect thermal diffusion so that the change of temperature $T(x,t)$ is given by

$$\dot{T}(x,t) = \frac{1}{\rho(x,t)c(x)}\dot{Q}(x,t), \tag{2.4}$$

where $c(x)$ is the specific heat capacity (i.e., the amount of energy needed to heat up a unit mass of the material by one unit of temperature) and $\rho(x,t)$ is the mass density.

Before we continue with our modeling equation, let us give a rough quantitative estimate of practically realizable temperature changes. We use the standard SI-units cm, m for centimeters and meters, μs for microseconds, g for grams, Ω for ohm, A for ampere, MHz for megahertz, J for joule, and mK, K, for millikelvin and kelvin. For the specific heat capacity and density we take the values of breast fat from Robinson, Richardson, Green and Preece [24, Table 5], $c = 2.43\mathrm{J}/(\mathrm{gK})$ and $\rho = 0.934\mathrm{g}/\mathrm{cm}^3$. The specific electrical conductivity of adipose tissue at a frequency of 1MHz is about $\sigma = 0.4/(\Omega\mathrm{m})$, cf., [27, Fig. 5]. Thus, a specimen cube of 1cm side length has a mass of $M = 0.934\mathrm{g}$ and its electrical resistance is $R = \sigma^{-1}\frac{\text{length}}{\text{area}} = 250\Omega$. Applying a pulse of $\Delta t = 1\mu\mathrm{s}$ with $\sigma|\nabla u| = I = 3\mathrm{A}$ will change the temperature of this cube by

$$\Delta T = \frac{1}{M}\frac{1}{c}RI^2\Delta t \approx 990\frac{\mathrm{K}\,\Omega\,\mathrm{A}^2\,\mu\mathrm{s}}{\mathrm{J}} = 0.99\,\mathrm{mK}\,.$$

This temperature raise seems enough to produce ultrasound waves, which can be measured with ultrasound transducers while still being unharmful to biological tissue.

We now proceed as in the derivation of the equations of thermoacoustic tomography in the book of Scherzer et al. [26], cf. also the publication of Haltmeier, Schuster and Scherzer [10], or the recent review article of Xu and Wang [28]. The change of the material's temperature can be related to the change of its density ρ and to the change of its pressure p via the so-called (linearized) expansion equation

$$\beta(x)\dot{T}(x,t) = \frac{1}{v_s^2}\dot{p}(x,t) - \dot{\rho}(x,t), \tag{2.5}$$

where v_s is the speed of sound and $\beta(x)$ is the thermal expansion coefficient that specifies the increase of volume per increase of temperature. Under the assumption

that the density ρ is only slightly varying from a constant value ρ_0 and only small velocities occur, the velocity v and the density ρ are coupled by the linearized continuity equation

$$\dot{\rho}(x,t) = -\rho_0 \nabla \cdot v(x,t). \tag{2.6}$$

Furthermore assuming an inviscid, non-turbulent flow of material with just slightly varying pressure, the velocity v is related to the pressure p by the linearized Euler equation

$$\rho_0 \dot{v}(x,t) = -\nabla p(x,t). \tag{2.7}$$

Combining (2.3)–(2.7) and applying again our assumption that that the density ρ is only slightly varying from ρ_0, we obtain

$$\frac{1}{v_s^2}\ddot{p}(x,t) - \Delta p(x,t) = \frac{\beta(x)}{\rho_0 c(x)}\sigma(x)|\nabla u(x)|^2 \dot{g}(t).$$

If the electric energy is only applied for a very short time (compared to the speed of sound) we can replace $g(t)$ by a δ-peak and obtain that p is the solution of

$$\begin{aligned} \frac{1}{v_s^2}\ddot{p}(x,t) - \Delta p(x,t) &= 0 && \text{in } \mathbb{R}^n, \\ p(x,0) &= \frac{\beta(x)}{\rho_0 c(x)}\sigma(x)|\nabla u(x)|^2 \chi_B(x) && \text{in } \mathbb{R}^n, \\ \dot{p}(x,0) &= 0 && \text{in } \mathbb{R}^n, \end{aligned}$$

where χ_B is the characteristic function of B. We furthermore assume that the specific heat capacity and the thermal expansion coefficient are approximately constant and known. By a standard change of units we can then eliminate v_s, β, ρ_0 and c from the equations and obtain together with (2.1) and (2.2) the *equations of impedance-acoustic tomography*,

$$\begin{aligned} \nabla \cdot \sigma \nabla u(x) &= 0 && \text{in } B, && (2.8) \\ u(x)|_S &= f && \text{on } S, && (2.9) \\ \ddot{p}(x,t) - \Delta p(x,t) &= 0 && \text{in } \mathbb{R}^n, && (2.10) \\ p(x,0) &= \sigma(x)|\nabla u(x)|^2 \chi_B(x) && \text{in } \mathbb{R}^n, && (2.11) \\ \dot{p}(x,0) &= 0 && \text{in } \mathbb{R}^n. && (2.12) \end{aligned}$$

The *forward problem of impedance-acoustic tomography* can now be stated as follows: Given the conductivity σ and the applied voltage f on S determine the resulting currents $\sigma\partial_\nu u|_S$ and the resulting pressure wave $p(x,t)$ that solves (2.8)–(2.12). The *inverse problem of impedance-acoustic tomography* consists of reconstructing the conductivity σ from knowledge of the applied voltage f and measurements of the resulting currents $\sigma\partial_\nu u|_S$ and the resulting pressure wave p on some part of $\mathbb{R}^3$. In this work we will restrict ourselves to the case where p is measured on the whole surface S for some time interval $[0,T]$ and we will furthermore assume that σ is known in a small neighborhood of this surface S.

Finishing this subsection, let us recapitulate the crucial assumptions regarding the time-scale in our model and give a rough estimate of feasible parameters. The applied voltage must vary slowly in time compared to the speed of electromagnetic waves, so that the (quasi-static) equations of impedance tomography are valid. The maximum frequency of Rensselaer's ACT 4 EIT system is 1MHz, cf. Saulnier, Liu, Tamma, Xia, Kao, Newell, and Isaacson [25]. At the same time, the voltage must only be applied for such a small time that thermal diffusion can be neglected and that the applied energy takes the form of a delta-pulse in the time-scale of sound waves, i.e., that also stress propagation can be neglected during the application of the pulse. The latter two conditions are commonly referred to as *thermal and stress confinements* in thermoacoustic tomography, cf. Xu and Wang [28]. The stress confinement is the more stringent condition and, for a pulse of 1μs, limits the expected spatial resolution to 1.5mm, cf. [28].

2.2. Well-posedness of the direct problem. Throughout this work we will assume that $B \subset \mathbb{R}^n$, $n = 2$ or $n = 3$, is a smoothly bounded domain, $T > 0$, $f \in W^{7/4,4}(S)$ and $\sigma \in W_+^{1,\infty}(B)$, where the subscript $+$ denotes the subspace of functions with positive essential infima. Under this assumption we obtain

LEMMA 2.1. *For every $\sigma \in W_+^{1,\infty}(B)$, there exists a unique solution $u \in W^{2,4}(B)$ of (2.8) and (2.9). Setting*

$$\mathcal{E}(\sigma) := \sigma|\nabla u|^2, \quad \text{where } u \text{ solves (2.8) and (2.9)}$$

defines a mapping $\mathcal{E} : W_+^{1,\infty}(B) \to H^1(B)$.

Proof. Note that the space $W^{7/4,4}(S)$ is the space of traces of functions from $W^{2,4}(B)$. From standard regularity results for elliptic equations, we obtain that for every $\sigma \in W_+^{1,\infty}(B)$ there exists a unique solution $u \in W^{2,4}(B)$ of (2.8) and (2.9) (cf., e.g., Miranda [21, Thm. 38,VI.]). Thus the result follows from the product rule for Sobolev functions. □

Some caution has to be taken in the treatment of the acoustic equations (2.10)-(2.12). Though we have just seen that our regularity assumptions guarantees that the initial condition is a H^1-function in B, its continuation by zero to $\mathbb{R}^n$ will in general have a jump across S. Roughly speaking, this jump persists in the pressure wave, so that our measurements $p|_S$ are in general not well-defined (as a function). Of course, from a practical point of view there cannot be an ambiguity in the measurement data, thus this problem shows that the idealization of a pressure wave appearing instantly in a sharply bounded body is not consistent with the idealization of a measurement surface with zero thickness.

However, using our additional assumption that we know the conductivity σ on S we can circumvent this problem without giving up one of these two idealizations. The quantity $\sigma(x)|\nabla u(x)|^2|_S$ can be calculated from $\sigma|_S$, the measured surface currents $\sigma(x)\partial_\nu u(x)|_S$ and the applied voltage $u(x)|_S = f(x)$. Using a function $\tilde{p}_0(x) \in H^1(B)$ with the same boundary values $\tilde{p}_0(x)|_S = \sigma(x)|\nabla u(x)|^2|_S$, we can define the solution $\tilde{p}$ of

$$\ddot{\tilde{p}}(x,t) - \Delta\tilde{p}(x,t) = 0 \qquad \text{in } \mathbb{R}^n, \tag{2.13}$$

$$\tilde{p}(x,0) = \tilde{p}_0(x)\chi_B(x) \qquad \text{in } \mathbb{R}^n, \tag{2.14}$$

$$\dot{\tilde{p}}(x,0) = 0 \qquad \text{in } \mathbb{R}^n. \tag{2.15}$$

The difference $q := p - \tilde{p}$ then solves the wave equation with an initial condition in $W^1(\mathbb{R}^n)$, and thus its trace on S is well-defined. Before we state this in a rigorous form below, let us comment on the practical realization of this approach. One can easily compute a smooth approximation to $\tilde{p}$ and evaluate this on S. The difference of the measurement of p on S and this quantity can then be regarded as an approximation to the well-defined, idealized model measurements $q|_S$.

We now restate the above arguments in a rigorous form.

LEMMA 2.2. *Denote by*

$$\gamma : \ H^1(B) \to H^{1/2}(S), \qquad v \mapsto v|_S,$$

the trace operator on S and let $\gamma^- : \ H^{1/2}(S) \to H^1(B)$ be a continuous right inverse of γ, i.e., $\gamma\gamma^- = Id$.

For every $\sigma \in W_+^{1,\infty}(B)$ there exists a unique solution $\tilde{p} \in C(0,T,L^2(\mathbb{R}^n))$ of (2.13)–(2.15) with $\tilde{p}_0 := \gamma^-\gamma\mathcal{E}(\sigma)$ and a unique solution $p \in C(0,T,L^2(\mathbb{R}^n))$ of (2.10) and (2.12) with $p(x,0) = \mathcal{E}(\sigma)\chi_B$. Their difference $q := p - \tilde{p}$ is an element of $C(0,T,W^1(\mathbb{R}^n))$ and it is the unique solution of

$$\ddot{q}(x,t) - \Delta q(x,t) = 0 \qquad \text{in } \mathbb{R}^n, \tag{2.16}$$

$$q(x,0) = q_0(x)\chi_B(x) \qquad \text{in } \mathbb{R}^n, \tag{2.17}$$

$$\dot{q}(x,0) = 0 \qquad \text{in } \mathbb{R}^n. \tag{2.18}$$

with $q_0 = (I - \gamma^-\gamma)\mathcal{E}(\sigma) \in H_0^1(B)$. Also, the mapping

$$\mathcal{F} : \ H_0^1(B) \to C(0,T,H^{1/2}(S)), \qquad q_0 \mapsto q|_S, \qquad \text{where } q \text{ solves (2.16)–(2.18),}$$

is continuous and linear.

Proof. This follows from classical results on the wave equation; cf., e.g., Lions and Magenes [18, Chp. 3, Thm. 9.3] for the unique existence of $\tilde{p}, p \in C(0,T,L^2(\mathbb{R}^n))$ and [18, Chp. 3, Thm. 8.2] for the unique existence of a solution $q \in C(0,T,W^1(\mathbb{R}^n))$ of (2.16)–(2.18). ∎

3. Inverse problems of ImpACT. In the last section we have seen that using the known boundary values of the conductivity $\sigma|_S$, the measured surface currents $\sigma(x)\partial_\nu u(x)|_S$ and the applied voltage $f(x)$ we can calculate $\gamma\mathcal{E}(\sigma) = \sigma|\nabla u|^2|_S$ and thus the *modified pressure measurements* $q|_S$ from the real measurement data. The dependance of $q|_S$ from the unknown conductivity σ is given by

$$q|_S = \mathcal{F}(I - \gamma^-\gamma)\mathcal{E}(\sigma).$$

Hence, the inverse problems of determining the conductivity from the measurements leads to the problems of inverting the two linear operators $\mathcal{F}$, $(I - \gamma^-\gamma)$ and the non-linear operator $\mathcal{E}$. Since $\gamma\mathcal{E}(\sigma)$ is known, the inversion of $(I - \gamma^-\gamma)$ consists simply of adding $\gamma^-\gamma\mathcal{E}(\sigma)$. It therefore remains to invert $\mathcal{F}$, i.e., to determine the initial value of a pressure wave from its trace on S, and to invert $\mathcal{E}$, i.e., to determine the conductivity of a body from its electrical energy density.

3.1. Determining the initial condition of the pressure wave. Recall that $\mathcal{F}: H_0^1(B) \to C(0,T,H^{1/2}(S))$ maps the initial value $q_0 \in H_0^1$ to the boundary values $q|_S$, where $q \in C(0,T,H^1(\mathbb{R}^n))$ solves

$$\begin{aligned} \ddot{q}(x,t) - \Delta q(x,t) &= 0 && \text{in } \mathbb{R}^n, \\ q(x,0) &= q_0(x)\chi_B(x) && \text{in } \mathbb{R}^n, \\ \dot{q}(x,0) &= 0 && \text{in } \mathbb{R}^n. \end{aligned}$$

The inverse problem of determining q_0 from $q|_S$ has been studied to some extent in the context of thermoacoustical tomography. We will use a conceptionally simple time-reversal algorithm that is also mentioned in the work of Finch, Patch and Rakesh [8, Thm. 5] and for which Burgholzer, Haltmeier, Matt and Paltauf show numerical results in the recent work [6]. Assume that $T > diam(B)$, then in the case of three spatial dimensions, the pressure wave q will have completely left the body B, so that $q(x,T)|_B = 0$ and $\dot{q}(x,T)|_B = 0$. Thus the time-reversed pressure wave $r(x,t) := q(x,T-t)|_B$ solves the initial boundary value problem,

$$\ddot{r}(x,t) - \Delta r(x,t) = 0 \quad \text{in } B, \tag{3.1}$$

$$r(x,t)|_S = g \quad \text{on } S, \tag{3.2}$$

$$r(x,0) = 0 \quad \text{in } B, \tag{3.3}$$

$$\dot{r}(x,0) = 0 \quad \text{in } B, \tag{3.4}$$

where the boundary data $g = q(x,T-t)|_S$ are just the time-reversed measurements.

LEMMA 3.1. *For every $g \in C(0,T,H^{1/2}(S))$, there exists a unique solution $r \in C(0,T,L^2(B))$ to the equations (3.1)–(3.4).*

Proof. Under the weaker assumption that $g \in L^2(0,T,L^2(S))$ this was shown by Lasiecka, Lions and Triggiani in [15, Thm. 2.3]. □

Since $q(x,T-t)$ solves (3.1)–(3.4), the initial condition $q(x,0)|_B = r(x,T)$ can thus be reconstructed from $q(x,t)|_S$ by solving (3.1)–(3.4) with $g = q(x,T-t)|_S$. Physically this can be interpreted as a combination of time-reversal of waves and the restriction to a bounded domain.

In the case of two spatial dimensions the wave does not leave the body completely, thus the solution of (3.1)–(3.4) will not completely agree with $q(x,T-t)$. However, if T is chosen large enough, then only a small part of the wave will still be in B, so that one can expect that the above method will still yield a good approximation to $q(x,0)$.

3.2. Determining the conductivity from the electrical energy. We now turn to the determination of the conductivity from the electrical energy, i.e, to the inversion of the non-linear mapping

$$\mathcal{E}: W_+^{1,\infty}(B) \to H^1(B), \qquad \sigma \mapsto \sigma(x)|\nabla u(x)|^2,$$

where u solves

$$\nabla \cdot \sigma \nabla u(x) = 0 \quad \text{in } B, \quad \text{and} \quad u|_S = f.$$

(Note we keep the applied voltage f fixed throughout this work.)

In [1], Ammari et al. reformulate this problem using the 0-Laplacian and propose an iterative reconstruction strategy that relies on the measurement of two different current patterns. We derive here a similar iterative scheme that is based on a formal Newton algorithm. Denote by u_σ the solution of

$$\nabla \cdot \sigma \nabla u = 0, \qquad u|_S = f.$$

It is well known (and easily shown) that (for $\operatorname{supp} \tau \subset B$) the directional derivative

$$v_\tau := \lim_{h \to 0} \frac{u_{\sigma + h\tau} - u_\sigma}{h}$$

is the solution of

$$\nabla \cdot \sigma \nabla v_\tau = -\nabla \cdot \tau \nabla u_\sigma, \qquad v|_S = 0. \tag{3.5}$$

It follows immediately that

$$\mathcal{E}'(\sigma)\tau = \tau |\nabla u_\sigma|^2 + 2\sigma \nabla u_\sigma \cdot \nabla v_\tau.$$

If $\hat{E} = \hat{\sigma}(x)|\nabla u_{\hat{\sigma}}(x)|^2$ is the reconstructed energy density and σ_n is an approximation to the true conductivity $\hat{\sigma}$, then a Newton-step would consist of solving

$$\mathcal{E}'(\sigma_n)\delta = \hat{E} - \sigma_n |\nabla u_{\sigma_n}(x)|^2$$

and the update $\sigma_{n+1} = \sigma_n + \delta$.

To get around the computationally expensive inversion of $\mathcal{E}'(\sigma)$, we can split it into two parts

$$\mathcal{E}'(\sigma)\tau = (M_\sigma + P_\sigma)\tau,$$

with

$$M_\sigma \tau := \tau |\nabla u_\sigma|^2 \quad \text{and} \quad P_\sigma \tau := 2\sigma \nabla u_\sigma \cdot \nabla v_\tau.$$

Apart from the problem that $|\nabla u|$ might be zero, the inversion of the multiplication operator M is computationally easy. Instead of using the exact inverse $(M_\sigma + P_\sigma)^{-1}$, one can use the approximate inverse $(I - M_\sigma^{-1} P_\sigma) M_\sigma^{-1}$, which is justified when $M_\sigma^{-1} P_\sigma$ is small. Notably, this approximation results in the same algorithm that Ammari et al. propose in [1] and that is therein motivated by a 0-Laplacian formulation:

Given $\hat{E}$, f and σ_n

- Calculate ∇u_{σ_n}
- Set $\tau := \dfrac{\hat{E}}{|\nabla u_\sigma|^2} - \sigma_n$.
- Calculate the solution v_τ of (3.5).
- Update $\sigma_{n+1} := \dfrac{\hat{E} - 2\sigma \nabla u_\sigma \cdot \nabla v_\tau}{|\nabla u_\sigma|^2}$.

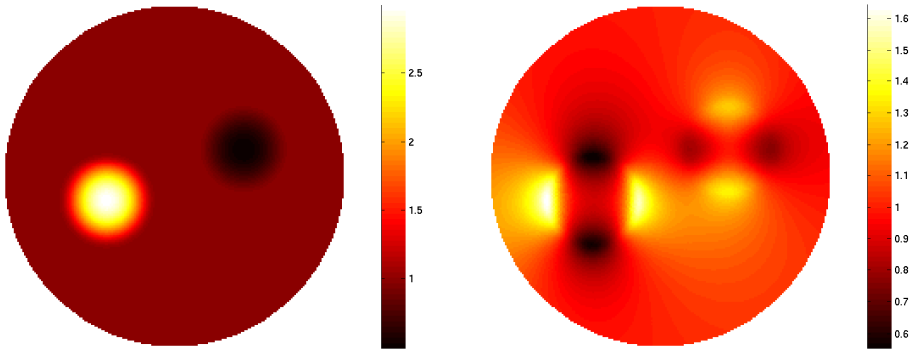

FIG. 4.1. *Exact conductivity and electrical energy distribution.*

4. Numerical examples. We have tested our inversion algorithm on simulated two-dimensional data. The left side of Figure 4.1 shows the exact conductivity distribution σ that we chose as our test example. A background conductivity of 1 is distorted by two discs centered at $(-0.4, -0.15)$ and $(0.4, 0.15)$ in which the conductivity is given by

$$1 + A_j \exp(R_j^{-1} - (R_j^2 - \rho_j^2)^{-1/2}), \quad j = 1, 2,$$

where $R_1 = R_2 = 0.3$ are the radii of the two discs, ρ_j is the respective distance to the center of the j-th disc, and $A_1 = 2$, $A_2 = 0.5$, so that the conductivity is smoothly raised to 3, resp., lowered to 0.5 inside the discs.

Using the commercial finite element software Comsol we calculated the corresponding electrical energy $\mathcal{E}(\sigma)$ and evaluated it using linear interpolation on the part of an equidistant 200×200 grid on $[-1, 1]^2$ that belongs to the unit circle. $\mathcal{E}(\sigma)$ is shown on the right side of Figure 4.1.

As the continuous right inverse γ^- of the trace operator we take the solution operator for the Dirichlet operator for the Laplace equation, which is implemented by expanding $\gamma\mathcal{E}(\sigma)$ into the L^2-orthonormal functions

$$\left\{ \frac{1}{\sqrt{2\pi}}, \frac{1}{\sqrt{\pi}} \sin(m\varphi), \frac{1}{\sqrt{\pi}} \cos(m\varphi) \;\middle|\; m = 1, \ldots, 100 \right\}$$

and using the analytical solutions for the corresponding Dirichlet problems

$$\left\{ \frac{1}{\sqrt{2\pi}}, \frac{1}{\sqrt{\pi}} \sin(m\varphi) r^m, \frac{1}{\sqrt{\pi}} \cos(m\varphi) r^m \;\middle|\; m = 1, \ldots, 100 \right\},$$

where (r, φ) denote the polar coordinates. Accordingly, the left side of Figure 4.2 shows the quantity $(I - \gamma^-\gamma)\mathcal{E}(\sigma)$.

The operator $\mathcal{F}$ is simulated by solving the wave equation with a standard central finite difference scheme on a sufficiently large domain. The values of q on the boundary S are then evaluated using linear interpolation on a equidistant grid on S. Thus, simulated (modified) measurements $q|_S$ are obtained.

We then tested our inversion algorithm on these simulated measurements. The Dirichlet problem for the wave equation was solved using the commercial finite element

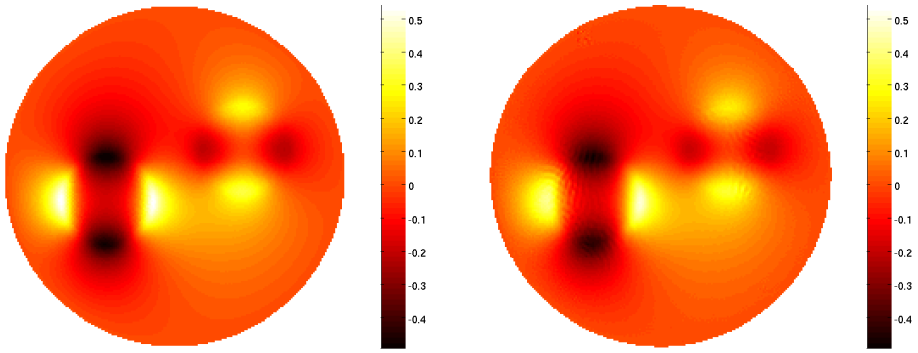

FIG. 4.2. *Exact and reconstructed (modified) energy distribution.*

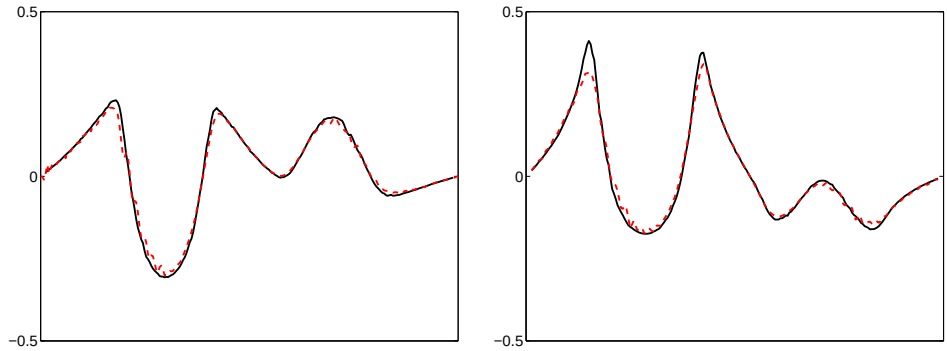

FIG. 4.3. *Profiles of exact and reconstructed (modified) energy.*

software Comsol. The reconstructed distribution $r(x,T)$, $T = 4$, is then evaluated using linear interpolation on the part of an equidistant 200×200 grid on $[-1,1]^2$ that belongs to the unit circle. Figure 4.2 compares the exact (modified) energy distribution $q(x,0) = (I - \gamma^- \gamma)\mathcal{E}(\sigma)$ (on the left side) with the reconstructed distribution $r(x,T)$, $T = 4$ (on the right side). Figure 4.3 shows profiles of the exact (solid black line) and of the reconstructed energy (dashed red line) on the x-axis (left plot) and on a line connecting the peaks of the true conductivity.

The known quantity $\gamma^- \gamma \mathcal{E}(\sigma)$ is then added to $r(x,T)$ and the Newton algorithm described in Section 3.2 is used on this data. As initial guess we used a constant conductivity of 1. The equations appearing in the Newton algorithm were again solved using the commercial finite element software Comsol. Note that thus the same finite element grid is used for the simulation of $\mathcal{E}$ as well as for its inversion. However, the energy is not given, resp., evaluated on this grid but on the independent equidistant grid described above, which minimizes the risk of an inverse crime. For the convenience of the reader we show on the left side of Figure 4.4 again the true conductivity to compare it with the best reconstruction that was obtained in the 24th Newton step (shown on the right side). We observed that the reconstructions do not improve afterwards which seems to be due to accumulated errors. Figure 4.5, which is organized in the same way as Figure 4.3, compares profiles of the true conductivity with the reconstruction.

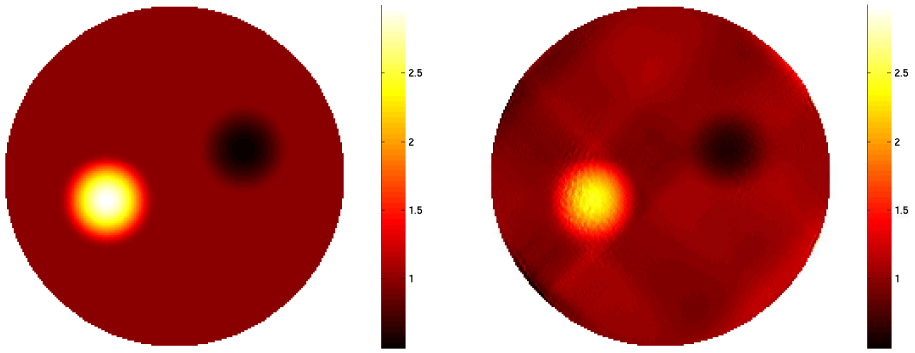

FIG. 4.4. *Exact and reconstructed conductivity distribution.*

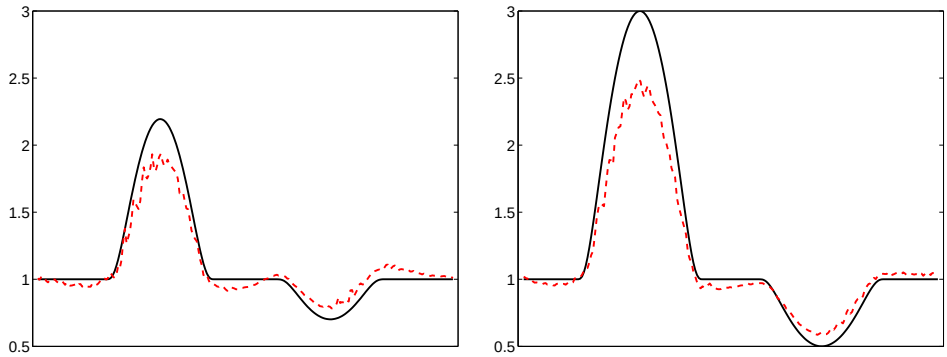

FIG. 4.5. *Profiles of exact and reconstructed conductivity.*

Acknowledgments. We thank Prof. Dr. Günther Paltauf from the University of Graz for advising us on the practical feasibility of our method and for providing us with information about high frequency surgery. OS also thanks Richard Kowar from the Infmath Imaging Group of the University of Innsbruck for support with physical quantities.

This work was conducted while BG was employed at the Johann Radon Institute for Computational and Applied Mathematics (RICAM), Austrian Academy of Sciences, Altenbergerstr. 69, A-4040 Linz, Austria.

The work of OS is supported by the Austrian Science Foundation, project NFN 10505.

REFERENCES

[1] H. AMMARI, E. BONNETIER, Y. CAPDEBOSCQ, M. TANTER AND M. FINK, *Electrical impedance tomography by elastic deformation*, SIAM J. Appl. Math. 68 (2008), 1557–1573.

[2] H. AMMARI, Y. CAPDEBOSCQ, H. KANG AND A. KOZHEMYAK *Mathematical models and reconstruction methods in magneto-acoustic imaging*, preprint available online at `http://hal.inria.fr/docs/00/28/85/29/PDF/ACKK_MAT_07_final.pdf`

[3] R. H. BAYFORD, *Bioimpedance tomography (electrical impedance tomography)* Annu. Rev. Biomed. Eng. 8 (2006), 63–91.

[4] L. BORCEA, *Electrical impedance tomography*, Inverse Problems, 18 (2002), pp. R99–R136.

[5] L. BORCEA, *Addendum to 'Electrical impedance tomography'*, Inverse Problems, 19 (2003), pp. 997–998.

[6] P. Burgholzer, M. Haltmeier, G. J. Matt and G. Paltauf, *Exact and approximative imaging methods for photoacoustic tomography using an arbitrary detection surface*, Physical Review E, 75 (2007), 046706-1.
[7] M. Cheney, D. Isaacson and J. C. Newell, *Electrical impedance tomography*, SIAM Rev., 41 (1999), pp. 85–101.
[8] D. Finch, S. K. Patch and Rakesh, *Determining a function from its mean values over a family of spheres*, SIAM J. Math. Anal., 35 (2004), pp. 1213–1240.
[9] R. Haag, *Hochfrequenzchirurgie*, in [13], pp. 396–411 (2002).
[10] M. Haltmeier, T. Schuster and O. Scherzer, *Filtered backprojection for thermoacoustic computed tomography in spherical geometry*, Math. Meth. Appl. Sci., 28 (2005), pp. 1919–1937.
[11] Y. J. Kim, O. Kwon, J. K. Seo, and E. .J. Woo, *Uniqueness and convergence of conductivity image reconstruction in magnetic resonance electrical impedance tomography*, Inverse Problems, 19 (2003), pp. 1213–1225.
[12] S. Kim, O. Kwon, J. K. Seo and J. R. Yoon, *On a nonlinear partial differential equation arising in magnetic resonance electrical impedance tomography*, SIAM J. Math. Anal., 34 (2003), pp. 511–526.
[13] R. Kramme, *Medizintechnik: Verfahren - Systeme - Informationsverarbeitung*, 2nd Edition Springer-Verlag, 2002.
[14] O. Kwon, E. J. Woo, J.-R. Yoon; J. K. Seo, *Magnetic resonance electrical impedance tomography (MREIT):simulation study of J-substitution algorithm*, IEEE Transactions on Biomedical Engineering, 49 (2002), pp. 160 - 167.
[15] I. Lasiecka, J.-L. Lions and R. Triggiani, *Non homogeneous boundary value problems for second order hyperbolic operators*, J. Math. Pures Appl., 65 (1986), pp. 149–192.
[16] M. Lazebnik, L. McCartney, D. Popovic, C. B. Watkins, M. J. Lindstrom, J. Harter, S. Sewall, A. Magliocco, J. H. Booske, M. Okoniewski and S. C. Hagness *A large-scale study of the ultrawideband microwave dielectric properties of normal breast tissue obtained from reduction surgeries*, Phys. Med. Biol., 52 (2007), pp. 2637–2656.
[17] M. Lazebnik, D. Popovic, L. McCartney, C. B. Watkins, M. J. Lindstrom, J. Harter, S. Sewall, T. Ogilvie, A. Magliocco, T. M. Breslin, W. Temple, D. Mew, J. H. Booske, M. Okoniewski and S. C. Hagness *A large-scale study of the ultrawideband microwave dielectric properties of normal, benign and malignant breast tissues obtained from cancer surgeries*, Phys. Med. Biol., 52 (2007), pp. 6093–6115.
[18] J. L. Lions and E. Magenes, *Non-homogeneous Boundary Value Problems and Applications I*, vol. 181 of Grundlehren Math. Wiss., Springer-Verlag, Berlin Heidelberg New York, 1972.
[19] W. R. B. Lionheart, *EIT reconstruction algorithms: pitfalls, challenges and recent developments*, Physiol. Meas. 25 (2004), pp. 125–142.
[20] Q. Ma and B. He, *Investigation on magnetoacoustic signal generation with magnetic induction and its application to electrical conductivity reconstruction* Phys. Med. Biol. 52 (2007), pp. 5085-5099.
[21] C. Miranda, *Partial differential equations of elliptic type*, vol. 2 of Ergeb. Math. Grenzgeb., Springer-Verlag, Berlin, 1970.
[22] A. Nachman, A. Tamasan and A. Timonov, *Conductivity imaging with a single measurement of boundary and interior data*, Inverse Problems, 23 (2007), pp. 2551-2563.
[23] S. K. Patch and O. Scherzer, eds, *Special section on photo- and thermoacoustic imaging*, Inverse Problems, 23 (2007), pp. S1-S122.
[24] M. P. Robinson, M. J. Richardson, J. L. Green and A. W. Preece, *New materials for dielectric simulation of tissues* Phys. Med. Biol. 36 (1991), pp. 1565–1571.
[25] G. J. Saulnier, N. Liu, C. Tamma, H. Xia, T. Kao, J. C. Newell and D. Isaacson, *An electrical impedance spectroscopy system for breast cancer detection*, Engineering in Medicine and Biology Society, 2007. EMBS 2007. 29th Annual International Conference of the IEEE, (2007), pp. 4154–4157.
[26] O. Scherzer, M. Grasmaier, H. Grossauer, M. Haltmeier and F. Lenzen *Variational Methods in Imaging*, Springer, New York, to appear.
[27] M. R. Stoneman, M. Kosempa, W. D. Gregory, C. W. Gregory, J. J. Marx, W. Mikkelson, J. Tjoe and V. Raicu, *Correction of electrode polarization contributions to the dielectric properties of normal and cancerous breast tissues at audio/radiofrequencies*, Phys. Med. Biol., 52 (2007), pp. 6589–6604.
[28] M. Xu and L. Wang *Photoacoustic imaging in biomedicine*, Rev. Sci. Instrum., 77, 041101 (2006).